

1 **Title:** Adaptively introgressed Neandertal haplotype at the OAS locus functionally  
2 impacts innate immune responses in humans.

3 **Authors**

4 Aaron J. Sams<sup>1,\*†</sup>, Anne Dumaine<sup>2†</sup>, Yohann Nédélec<sup>2,3†</sup>, Vania Yotova<sup>2</sup>, Caroline  
5 Alfieri<sup>2,4</sup>, Jerome E. Tanner<sup>2</sup>, Philipp W. Messer<sup>1\*\*†</sup>, and Luis B. Barreiro<sup>2,5,\*\*†</sup>

6 **Affiliations**

7 <sup>1</sup>Department of Biological Statistics and Computational Biology, Cornell  
8 University, Ithaca, NY

9 <sup>2</sup>Department of Genetics, Sainte-Justine Hospital Research Centre, University of  
10 Montreal, Montreal, Qc, Canada

11 <sup>3</sup>Department of Biochemistry, University of Montreal, Montreal, Qc, Canada

12 <sup>4</sup>Department of Microbiology and Immunology, University of Montreal, Montreal,  
13 Qc, Canada

14 <sup>5</sup>Department of Pediatrics, University of Montreal, Montreal, Qc, Canada

15 <sup>†</sup>These authors contributed equally to this work

16 <sup>\*\*†</sup>These authors jointly supervised this work

17 \*Correspondence to: (A.J.S.) [as2847@cornell.edu](mailto:as2847@cornell.edu), (P.W.M.) [messer@cornell.edu](mailto:messer@cornell.edu),  
18 (L.B.B.) [luis.barreiro@umontreal.ca](mailto:luis.barreiro@umontreal.ca)

19 **Abstract**

20 The 2'-5' oligoadenylate synthetase (OAS) locus encodes for three OAS enzymes  
21 (OAS1-3) involved in innate immune response. This region harbors high amounts  
22 of Neandertal ancestry in non-African populations; yet, strong evidence of positive  
23 selection in the OAS region is still lacking. Here we used a combination of neutral  
24 coalescent simulations and neutrality tests to firmly demonstrate a signal of  
25 adaptive introgression at the OAS locus. Furthermore, we characterized the  
26 functional consequences of the Neandertal haplotype in the transcriptional  
27 regulation of OAS genes at baseline and infected conditions. We found that cells  
28 from people with the Neandertal-like haplotype express lower levels of *OAS3*  
29 upon infection, as well as distinct isoforms of *OAS1* and *OAS2*. Notably, the  
30 Neandertal-introgressed haplotype reintroduced an ancestral splice variant of  
31 *OAS1* encoding a more active protein, suggesting that adaptive introgression  
32 occurred as a means to resurrect adaptive variation that had been lost outside  
33 Africa.

34 **Introduction**

35 Whole genome sequencing of several archaic human genomes (Green et al., 2010;  
36 Reich et al., 2010; Meyer et al., 2012; Prüfer et al., 2014; Sawyer et al., 2015)  
37 representing Neandertals and an as yet geographically and paleontologically  
38 unknown population referred to as Denisovans has revealed gene flow between  
39 these populations and the ancestors of present-day humans. Neandertal ancestry  
40 makes up approximately 0.5-2 percent of the ancestry of most living humans, with

41 higher amounts of Neandertal ancestry found outside of Africa(Sankararaman et  
42 al., 2014; Vernot and Akey, 2014; Llorente et al., 2015). While it seems that there  
43 may have been widespread purifying selection against Neandertal ancestry on the  
44 ancestral African genomic background(Sankararaman et al., 2014; Vernot and  
45 Akey, 2014), some positive selection on Neandertal genes (adaptive introgression)  
46 has also been observed(Racimo et al., 2015; 2016). Neandertals and other archaic  
47 populations inhabited Eurasia for several hundred thousand years(Hublin, 2009),  
48 therefore some adaptive introgression is expected, particularly across phenotypes  
49 that are strongly influenced by direct interactions with the surrounding  
50 environment (Racimo et al., 2015), such as our immune response to infectious  
51 agents (Ségurel and Quintana-Murci, 2014).

52 The OAS locus on chromosome 12, which harbors three genes (*OAS1*, *OAS2*,  
53 *OAS3*) encoding the 2'-5' oligoadenylate synthetase enzymes has received  
54 considerable attention due to its clear signs of multiple archaic haplotypes in  
55 populations outside of Africa(Mendez et al., 2012; 2013), and the critical role of  
56 OAS genes in the innate immune response to viruses (Player and Torrence, 1998).  
57 The major Neandertal haplotype at the OAS locus spans a ~190 kilobase region  
58 between two surrounding recombination hotspots. This haplotype is absent from  
59 sub-Saharan African samples in the 1000 Genomes Project data, yet found at  
60 relatively high frequencies outside of Africa, reaching highest frequencies in  
61 European population samples (up to 41%, Figure 1). Indeed, the Neandertal  
62 haplotypes in the OAS region are among the most common Neandertal haplotypes  
63 among Europeans(Sankararaman et al., 2014).

64 The elevated frequency of the introgressed haplotype along with the key role OAS  
65 genes play in protective immunity against viral infections raises the possibility that  
66 introgressed Neandertal haplotypes at OAS may have been adaptive in modern  
67 humans. While some studies provide suggestive evidence of adaptive introgression  
68 at the OAS locus (Sankararaman et al., 2014; Racimo et al., 2016), strong  
69 evidence of positive selection in the OAS region is still lacking. Indeed, most  
70 studies failed to reject a model of neutral evolution for the Neandertal haplotype  
71 when using standard neutrality tests (Mendez et al., 2013; Deschamps et al., 2016).  
72 We hypothesize that the overall lack of signals of selection in the OAS region  
73 stems from the low power of standard neutrality tests to detect adaptive  
74 introgression (Sankararaman et al., 2016), and the particular genomic architecture  
75 of the region, which is characterized by the presence of two strong recombination  
76 hotspots (Figure 2A). The presence of these recombination hotspots is likely to  
77 significantly reduce power to detect signals of selection, particularly for tests  
78 based on haplotype-lengths or levels of linkage disequilibrium associated with the  
79 selected allele. Here we circumvent these issues by testing the hypothesis of  
80 adaptive introgression using extensive neutral coalescent simulations specifically  
81 tailored to match the genomic features of the OAS region in combination with  
82 ancient DNA data from Eurasia. We firmly demonstrate a population genetic  
83 signal of adaptive introgression at the OAS locus and characterize the functional  
84 consequences of the Neandertal haplotype in the transcriptional regulation of OAS  
85 genes in macrophages and peripheral blood mononuclear cells (PBMCs) at  
86 baseline and infected conditions.

## 87 **Results**

88 To investigate the hypothesis of non-neutral evolution at the OAS locus we  
89 simulated neutral sequence data using a demographic model based on several  
90 previously inferred parameters of human demographic history(Gravel et al., 2011;  
91 Tennessen et al., 2012; Vernot and Akey, 2015)(Figure S1) and explicitly  
92 incorporated estimated recombination rates in the OAS region (Methods). Our  
93 model included a single pulse of Neandertal introgression occurring over a span of  
94 500-1000 years (sampled from a uniform distribution) into the ancestral Eurasian  
95 population after their population split from Africa. We investigated patterns of  
96 haplotype homozygosity surrounding Neandertal-like sites (NLS), derived alleles  
97 that are shared between Neandertals and a non-African population sample (CEU),  
98 but absent in a sub-Saharan African sample (YRI). This class of sites is frequently  
99 used as a conservative indicator of Neandertal introgression(Yang et al., 2012; Fu  
100 et al., 2014; Sankararaman et al., 2014). In each simulation we chose a NLS at  
101 random to measure two summary statistics, NLS frequency, and  $H_{D/A}$ , a statistic  
102 which measures the ratio of average pairwise homozygosity tract lengths among  
103 haplotypes carrying a derived versus ancestral allele at each NLS (Methods). This  
104 statistic is based on the  $H$  statistic that provides a general measure for haplotype  
105 lengths and has been shown to be robust in detecting both hard and soft selective  
106 sweeps(Schlamp et al., 2016). If Neandertal haplotypes have experienced a greater  
107 rate of positive selection than ancestral haplotypes, this should lead to a relative  
108 increase of  $H$  among the subgroup of haplotypes that carry Neandertal alleles  
109 versus those carrying only ancestral alleles, leading to higher values of  $H_{D/A}$

110 compared to a neutrally evolving locus with similar recombination rates (Figure  
111 S2). Additionally, we expected the frequency of NLS at the OAS locus to be  
112 elevated compared to the NLS frequency distribution observed across neutral  
113 simulations.

114 In practice, we observed both signals. We first examined the probability in our  
115 model that neutrally evolving Neandertal like sites would be segregating at their  
116 current frequencies. We found that the highest frequency NLS (DAF = 38.4%) fall  
117 in the extreme 1% of all simulations (lowest  $P = 0.0055$ ) (Figure 2A). Next, we  
118 compared  $H_{D/A}$  at each NLS in the OAS region to distributions of simulated NLS  
119 drawn to match local recombination rate and frequency (Methods), thereby  
120 controlling for associations between frequency and recombination, and haplotype  
121 lengths. We found several NLS in the OAS region that have  $H_{D/A}$  values greater  
122 than 99% of comparable simulated NLS (lowest  $P = 0.0023$ ) (Figure 2B). Further,  
123 we measured mean  $H_{D/A}$  across all NLS in the OAS region and compared this to  
124 randomly sampled distributions of simulated NLS (again matching frequency and  
125 recombination rate). We found that the true mean  $H_{D/A}$  in OAS is greater than four  
126 standard errors from the neutral expectation ( $P < 10^{-5}$ ) (Figure 2D). Lastly, we  
127 considered the joint probability of observing a neutral NLS in our simulations with  
128 frequencies and  $H_{D/A}$  values as high as those observed in the OAS region. Only  
129 413 simulated NLS (out of 1,000,079) had both a higher frequency and  $H_{D/A}$  value  
130 than the highest frequency/  $H_{D/A}$  pair in our NLS sample ( $P < 5 \times 10^{-4}$ ) (Figure 2E).  
131 Combined, we identified the strongest evidence to date in support of adaptive  
132 introgression in the OAS region.

133 We further supported and contextualized our simulation results by examining the  
134 OAS region in a dataset of 230 ancient Eurasians(Mathieson et al., 2015).  
135 Assuming neutrality, the expected frequency of an allele in contemporary  
136 European populations can be predicted as a linear combination of allele  
137 frequencies sampled from representative ancient populations that have contributed  
138 ancestry to present-day European populations in different proportions(Lazaridis et  
139 al., 2014; Mathieson et al., 2015) (Methods). Therefore, using ancient allele  
140 frequencies estimated by Mathieson and colleagues, we calculated the expected  
141 allele frequency in four present day European samples from the 1,000 Genomes  
142 Project(Consortium, 2015) at 11 NLS falling within the bounds of the three OAS  
143 genes. To set up our null expectations we performed a similar analysis on a dataset  
144 of approximately one million SNPs scattered around the genome, generated by  
145 Mathieson and colleagues (by merging 213 ancient samples dated between 6500  
146 and 300 BCE with sequencing data from four European samples from the 1,000  
147 Genomes Project). We found that OAS NLS SNPs are outliers in the genome with  
148 respect to deviations from ancient frequencies. More specifically, we found that  
149 the allele frequency of 6 out of the 11 OAS SNPs tested in the *OAS1-OAS3* region  
150 have increased above the frequency predicted by ancient Eurasian samples by  
151 more than 20%, significantly more than what we observed for other SNPs  
152 genome-wide with comparable present-day frequencies (lowest  $P = 0.00476$ ,  
153 Figure 2C, Table S1). Our findings at this single locus are consistent with results  
154 from the genome-wide selection scan performed by Mathieson and  
155 colleagues(2015) where the OAS region was also identified as an outlier.

156 Our population genetic results provide evidence that Neandertal alleles at the OAS  
157 locus have likely experienced positive selection at some point after their  
158 introduction into the human population, suggesting a possible functional role of  
159 these alleles in human innate immune responses. To study this possibility, we  
160 analyzed RNA-sequencing data collected on primary macrophages from 99  
161 European-descent individuals, before and after *in-vitro* infection with *Salmonella*  
162 *typhimurium*. After 2 hours of infection, we found that all OAS genes were  
163 strongly up-regulated (up to 19-fold,  $P < 1 \times 10^{-10}$ , Figure S3), confirming the  
164 ability of *Salmonella* to activate the interferon (IFN) production pathway (Nauciel  
165 and Espinasse-Maes, 1992; Gulig et al., 1997; LaRock et al., 2015). Using  
166 genotype data available for the same individuals (673 SNPs spanning the OAS  
167 region, see methods) we tested if NLS were associated with variation in the  
168 expression levels of *OAS1*, *OAS2* or *OAS3*, in either infected or non-infected  
169 macrophages. We found that SNPs linked with the Neandertal haplotype impacted  
170 the expression levels of *OAS3* (i.e., they were expression quantitative trait loci, or  
171 *cis* eQTL for *OAS3*) (Figure 3A, false discovery rate (FDR) < 5%). Interestingly,  
172 these *cis* eQTL showed a much stronger effect in infected macrophages (best  $P$   
173 *salmonella* =  $3.5 \times 10^{-3}$  vs best  $P_{\text{non-infected}}$  = 0.027), supporting an interaction between  
174 the Neandertal haplotype and the *OAS3* response to *Salmonella* infection.

175 In addition to overall changes in expression, we took advantage of the power of  
176 RNA-sequencing data to test if NLS in the OAS regions influenced the ratio of  
177 alternative isoforms used for each of the OAS genes (i.e., alternative splicing  
178 QTL: asQTL). We found that SNPs associated with the Neandertal haplotype are



179 significant asQTL for *OAS1* and *OAS2* in both infected and non-infected  
180 macrophages (FDR $\ll$  1%; Figure 3B-C). The effect of the splice site variant  
181 rs10774671 at determining what isoform is primarily encoded by *OAS1* was  
182 particularly strong ( $P \leq 2 \times 10^{-32}$ ). The ancestral G allele at this SNP (AG at  
183 acceptor site) retains the splice site whereas the derived allele, A, (AA at acceptor  
184 site) disrupts the splice site leading to the usage of a distinct isoform (Figure S4).  
185 The Neandertal haplotype harbors the ancestral allele (encoding the p46 isoform),  
186 which is associated with high enzyme activity (Bonnievie-Nielsen et al., 2005),  
187 whereas the derived allele – present in virtually all non-Neandertal haplotypes  
188 found outside Africa (98.4% in CEU) – is associated with reduced enzymatic  
189 activity.

190 Because OAS genes are primarily involved in the control of viral infections we  
191 decided to validate our functional findings on peripheral blood mononuclear cells  
192 (PBMCs) from 30 individuals stimulated/infected with viral-ligands (polyI:C and  
193 gardiquimod), and live viruses (Influenza, Herpes simplex virus (HSV) 1 and  
194 HSV2). The individuals were chosen based on their genotype for the NLS  
195 rs1557866, a SNP that is a strong proxy for the presence or absence of the  
196 Neandertal haplotype in the OAS region (9 were homozygous for the Neandertal  
197 haplotype, 9 were heterozygous, and 12 homozygous for the modern human  
198 sequence).

199 As expected, we found that all viral-associated immune triggers led to a marked  
200 increase in *OAS1-3* gene expression levels, as measured by real-time PCR (up to

201 30-fold,  $P \leq 5.4 \times 10^{-6}$ , Figure 4A), concomitantly with the up-regulation of type-I  
202 and type-II interferon genes (Figure S5). Confirming the QTL results obtained in  
203 macrophages, we found that rs10774671 was a strong asQTL for *OAS1* in both  
204 non-infected and infected PBMCs ( $P \leq 5.9 \times 10^{-5}$ , Figure 4B). Likewise, we found  
205 that the presence of the Neandertal haplotype was associated with increased  
206 expression levels of *OAS3*, particularly in PBMCs infected with influenza ( $P =$   
207 0.01) and the synthetic ligand gardiquimod ( $P = 4.0 \times 10^{-4}$ ), which mimics a single  
208 strand RNA infection (Figure 4B). Interestingly, the Neandertal haplotype harbors  
209 additional regulatory variants that only impact expression levels in a cell-type and  
210 immune stimuli specific fashion. For example, we found that the Neandertal  
211 haplotype is associated with increased expression levels of *OAS1* and *OAS2* in  
212 non-infected ( $P < 0.01$ ) and gardiquimod-stimulated PBMCs ( $P < 0.0004$ ), but not in  
213 macrophages nor in PBMCs treated with other viral agents. Collectively, our  
214 functional data shows a pervasive impact of the Neandertal haplotype on the  
215 regulation of *OAS* genes. Moreover, they show that the regulatory impact of the  
216 Neandertal haplotype varies depending on the cell type and the immune stimuli the  
217 cells are responding to.

## 218 **Discussion**

219 The Neandertal lineage was present in Eurasia for at least 400,000 years (Meyer et  
220 al., 2016), providing ample time for Neandertals to adapt to local disease  
221 environments. The admixture process, which likely fostered the transmission of  
222 pathogens between Neandertals and humans migrating out of Africa, could have

223 also led to the exchange of genes useful in responding to local pathogens. Here,  
224 we have demonstrated that a previously reported case of Neandertal introgression  
225 at the OAS locus (Mendez et al., 2013) displays signatures of positive selection in  
226 the European population. Additionally, we have strengthened the case for adaptive  
227 introgression by providing direct functional evidence of a role for the Neandertal  
228 OAS haplotype to the regulatory responses in innate immune cells to infectious  
229 agents.

230 Under a model of constant directional selection with codominant fitness effects for  
231 Neandertal alleles we can use present-day frequencies and a plausible  
232 establishment frequency at the time of introgression to estimate the selection  
233 coefficient associated with the Neandertal haplotype at the OAS locus (Methods).  
234 Assuming an establishment frequency of 0.02, and introgression approximately  
235 2000-2400 generations ago the selection coefficient in heterozygotes would be  $s \sim$   
236 0.0014 - 0.0017. However, the observed allele frequency shift of 0.26 in only 200-  
237 340 generations (maximum shift in CEU from ancient samples; see Figure 2C)  
238 predicts that the selection coefficient associated with the Neandertal haplotype was  
239 2.6-5.4 times larger during recent human evolution ( $s \sim 0.0044 - 0.0075$ ). These  
240 results suggest that the Neandertal OAS haplotype has not experienced constant  
241 directional selection in humans.

242 Our results show that the Neandertal haplotype at OAS is associated with several  
243 regulatory variants that reduce expression of *OAS3* in response to infection, as  
244 well as encode alternate isoforms of *OAS1* and *OAS2*. These dramatic functional

245 implications of the Neandertal OAS haplotype support our case for adaptive  
246 introgression at OAS. Yet, because distinct functional polymorphisms segregate  
247 together in the same haplotype, inferring the exact variant(s) targeted by positive  
248 selection remains a daunting task. We speculate, however, that the direct target of  
249 selection is likely to have been the splice variant identified in *OAS1*.

250 The Neandertal haplotype carries the ancestral allele (G) of the *OAS1* splice  
251 variant (rs10774671), which is common both inside and outside of Africa.  
252 However, outside of Africa, the only haplotypes carrying this ancestral splice site  
253 are closely related to the Neandertal haplotype, with a few exceptions being rare  
254 recombined haplotypes (~2% of all haplotypes with the ancestral allele). This  
255 pattern reflects the possibility that Neandertal introgression, in effect, served as a  
256 means to resurrect the ancestral splice site from local extinction outside of Africa,  
257 probably following the out-of-Africa exodus. The Neandertal-introgressed allele  
258 encodes a protein variant (p46) that is associated with higher enzymatic  
259 activity (Bonnievie-Nielsen et al., 2005). The adaptive potential of this variant is  
260 supported by the observation that this variant (or other variants in strong LD with  
261 it) was shown to be associated with: (i) reduced infection and replication rates of  
262 West Nile virus ((Lim et al., 2009), but see (Bigham et al., 2011)), (ii) improved  
263 resistance to hepatitis C virus (HCV) infection (Awady et al., 2011; Kwon et al.,  
264 2012), and (iii) variable symptomology of Tick-Borne Encephalitis (TBE) Virus-  
265 Induced Disease (homozygous individuals for the Neandertal haplotype show the  
266 most severe symptoms of TBE). Strikingly, West Nile, hepatitis C and TBE are

267 all members of the *Flaviviridae* family, suggesting that Flaviviruses might have  
268 been the main drivers of selection in *OAS1*.

269 The differential responses of homozygous carriers of the Neandertal OAS  
270 haplotype to the different viruses described above suggest that the Neandertal  
271 haplotype is not uniformly beneficial in humans. Thus, it is plausible that alleles at  
272 OAS, and particularly the *OAS1* splice variant, might be evolving under balancing  
273 selection. This hypothesis is supported by the observation that the *OAS1* splice  
274 variant (rs10774671) is found at high frequency worldwide (0.11-0.7), and that  
275 *OAS1* is among the most diverse genes in both humans and non-human primates.  
276 Indeed, a recent analysis of genome-wide sequence data from a total of 55  
277 individuals from four non-human ape species, chimpanzee (*Pan troglodytes*  
278 *elliotti*), bonobo (*Pan paniscus*), gorilla (*Gorilla gorilla gorilla*), and orangutan  
279 (*Pongo abelii*), identified *OAS1* as in the top 1% of genes showing the largest  
280 levels of nucleotide diversity among ape species, consistent with a scenario of  
281 long-term balancing selection (*OAS2* and *OAS3* are ranked in the 60th and 36th  
282 percentile of the genome-wide distribution, respectively). Further supporting the  
283 idea of balancing selection on the introgressed haplotypes, our functional data  
284 suggest that the Neandertal haplotype contributes a range of gene expression  
285 responses in a cell-type and stimulus-specific manner.

286 In conclusion, our study demonstrates that the frequency and haplotype  
287 distribution of Neandertal-like sites can be used in a neutral simulation framework  
288 that accounts for local genomic context to investigate the history of selection at a

289 candidate locus for which genome-wide tests of selection provide ambiguous  
290 results. When combined with functional data, our results provide the strongest  
291 evidence to date in support of adaptive introgression in the OAS region. More  
292 generally, our study raises the possibility that adaptive introgression might not  
293 necessarily occur to select newly introduced variants but rather as a means to  
294 resurrect adaptive variation into modern humans who had lost it due to  
295 demographic events.

## 296 **Materials and Methods**

### 297 *1. Genome alignments and identification of Neandertal-like sites*

298 Human/chimpanzee ancestral states were computed by parsimony using  
299 alignments from the UCSC Genome Browser for the human reference (hg19) and  
300 three outgroups chimpanzee (panTro2), orangutan (ponAbe2), and rhesus macaque  
301 (rheMac2)(Kent et al., 2002). Ancestral state was assumed to be the chimpanzee  
302 allele (if available) if its state was confirmed by matching either orangutan or  
303 macaque. All sites with no inferred ancestral state were removed from our  
304 analysis.

305 We filtered the Altai Neandertal genome(Prüfer et al., 2014) using the map35\_50  
306 set of minimum filters provided at  
307 ([https://bioinf.eva.mpg.de/altai\\_minimal\\_filters/](https://bioinf.eva.mpg.de/altai_minimal_filters/)). We combined this filtered  
308 dataset with the CEU (Utah residents (CEPH) with Northern and Western  
309 European Ancestry) and YRI (Yoruba in Ibadan, Nigeria) samples from the 1000

310 Genomes Project Phase 3(Consortium, 2015), which we downloaded from  
311 (<https://mathgen.stats.ox.ac.uk/impute/1000GP%20Phase%203%20haplotypes%206%20October%202014.html>).

313 We first extracted all variants that were biallelic in our human (CEU+YRI),  
314 Neandertal, and chimpanzee alignments. We considered as Neandertal-like sites  
315 (NLS) only those variants where the African sample (YRI) had a derived allele  
316 frequency of zero and both CEU and Neandertal carried the derived  
317 allele. Finally, we required the derived allele to be present in CEU in at least two  
318 copies in order to calculate our haplotype-based test statistic ( $H_{D/A}$ ).

## 319 *2. Demographic model and neutral coalescent simulations*

320 We performed coalescent simulations of the demographic history of the European,  
321 African, and Neandertal populations applied by Vernot and Akey(2015) based on  
322 previously inferred demographic models (Gravel et al., 2011; Tennessen et al.,  
323 2012) with some minor adjustments, including removing the East Asian  
324 component of the model and allowing for Neandertal admixture to occur over a  
325 time span from 500 to 1000 years (Figure S1). Simulations were performed with  
326 macs(Chen et al., 2009) in order to explicitly simulate the genetic map  
327 (downloaded with the 1000 Genomes samples at the link above) of the 2Mb region  
328 centered on OAS (chr12:112400000-114400000). All simulations were performed  
329 with the parameters specified in Figure S1, assuming 25 years per generation and a  
330 mutation rate of  $2.5 \times 10^{-8}$  per bp per generation. A sample macs command is  
331 given at the end of this section.

332 Data were thinned in a manner similar to Sankararaman et al. 2014 (2014) to  
333 account for imperfect SNP ascertainment in the 1000 Genomes dataset, such that  
334 SNPs with minor allele count of 1, 2, 3, 4, 5, 6, 7, 8, 9, and  $\geq 10$  were accepted  
335 with probabilities 0.25, 0.5, 0.75, 0.8, 0.9, 0.95, 0.96, 0.97, 0.98, and 0.99,  
336 respectively. Additionally, we only kept SNPs that were polymorphic in the  
337 simulated CEU sample. Finally, we performed an additional thinning of SNPs  
338 with uniform probability of 0.05 of removal to account for slightly elevated SNP  
339 density in the simulated data. The resulting simulated datasets had an average  
340 SNP density of 4.9 SNPs per kb compared to 3.6 in the real data. This is a slightly  
341 larger than ideal difference in SNP density, but we note that neither derived allele  
342 frequency, nor our primary haplotype-based test statistic (described below) should  
343 be particularly sensitive to SNP density. In fact, Figure S6 illustrates that our  
344 statistic is conservative with respect to SNP density.

345 To estimate the probabilities of adaptive introgression conditional on the simulated  
346 locus containing a NLS (SNPs in which the non-African and Neandertal sample  
347 contain a derived allele that is absent from the African sample) we randomly  
348 selected a single NLS from the central fifth of the chromosome (positions 0.4-0.6  
349 in the unit scaled locus) in which we calculated our test statistics. If an NLS was  
350 found, its position on the chromosome was recorded and test statistics were  
351 calculated. If no NLS was found, we repeated the simulation step. This approach  
352 allowed us to estimate under our demographic model, the proportion of  
353 independent loci that will have no obvious signal of introgression under neutrality  
354 as the proportion of successful simulation runs to the total number of attempts. We



355 obtained an approximate 21 percent chance of observing Neandertal introgression  
356 at the OAS locus under a neutral model. Additionally, we repeated this simulation  
357 approach, setting Neandertal introgression to zero, in a set of 10,000 simulations in  
358 order to estimate the likelihood of observing a NLS in the case of incomplete  
359 lineage sorting (ILS), to estimate the contribution of ILS to our null distribution.  
360 We observed a roughly 0.6% chance that a NLS is produced by ILS at the OAS  
361 locus, suggesting that our null distribution is not significantly biased by ILS.

362 Sample macs command:

```
363 macs 416 2000000 -t 0.000731 -R oas_recrates.txt -I 3 216 2 198 0 -n 1  
364 58.0027359781 -n 2 0.205198358413 -n 3 70.0410396717 -eg 0 1 482.67144247 -  
365 eg 1e-08 3 570.175408787 -em 2e-08 1 3 0.409323665059 -em 3e-08 3 1  
366 0.409323665059 -eg 0.00699726402189 3 16.9958723831 -en 0.00699727402189  
367 1 1.98002735978 -en 0.03146374829 3 0.759313629055 -en 0.0561902522706 3  
368 1.15461721321 -em 0.0561902622706 1 3 4.386 -em 0.0561902722706 3 1 4.386  
369 -em 0.056088019083 3 2 17.3006865925 -em 0.0569023606299 3 2 0.0 -ej  
370 0.08129305892 3 1 -en 0.08129306892 1 1.98002735978 -en 0.202462380301 1  
371 1.0 -ej 0.89014331235 2 1 -h 1e3 1e3
```

### 372 *3. Frequency and haplotype-based tests of neutrality*

373 We examined the consistency of genetic variation with our neutral model using  
374 several approaches. First, we examined the likelihood of observing (Neandertal)  
375 allele frequencies as high as the OAS locus. Under neutrality, allele frequency is

376 not dependent upon recombination rate, therefore, we can estimate the likelihood  
377 of our observed NLS frequency in the OAS region. For example, mean allele  
378 frequency of all NLS observed between chr12:113344000-113450000 is 0.35  
379 (Figure 2A). Frequencies this great or greater were observed in our simulations  
380 less than one percent of the time (0.0085), suggesting that this haplotype  
381 frequency is unlikely under neutrality.

382 Additionally, we wanted to examine if the haplotypes carrying NLS at the OAS  
383 locus are longer than expected under neutrality when conditioning on the observed  
384 frequencies and the underlying genetic map, which would provide an additional  
385 signature of selection on introgressed haplotypes. For this purpose, we modified a  
386 simple haplotype statistic  $H$  (Schlamp et al., 2016), which measures the average  
387 length of pairwise homozygosity tracts in base pairs – a quantity that is very  
388 straightforward to interpret. As selective sweeps are expected to create long  
389 haplotypes around the selected site, the  $H$  statistic should be higher in samples  
390 containing positively selected haplotypes compared to samples containing  
391 neutrally evolving haplotypes, when frequency and recombination are properly  
392 controlled, similar to other statistics based on haplotype lengths, such as  $EHH$ ,  
393  $iHS$ , and  $nSL$  (Sabeti, P.C. et al., 2002; Voight et al., 2006; Ferrer-Admetlla et al.,  
394 2014). However, in contrast to these other statistics,  $H$  does not require  
395 specification of analysis parameters such as minimum haplotype homozygosity  
396 levels below which haplotypes are no longer extended.

397 Under adaptive introgression, we specifically expect the introgressed haplotypes to  
398 be longer than the ancestral haplotypes. We therefore defined our test statistic,  
399  $H_{D/A}$ , as:

$$400 \quad H_{D/A} = \ln(H_D/H_A);$$

401 where  $H_D$  and  $H_A$  are  $H$  calculated across haplotypes carrying derived NLS allele  
402 versus the ancestral allele.

403 We calculated this statistic for every simulated NLS and for every NLS in our true  
404 sample. We compared our simulation results to the observed data in two  
405 ways. First, for each observed SNP we gathered all simulated NLS within 0.025  
406 frequency and 20 kb. We then calculate the empirical likelihood of observing  
407 each observed NLS under our neutral demographic model (Figure 2A). All NLS  
408 within the bounds of the three OAS genes are tightly linked, therefore, the peak  
409 signal at the center of this locus suggests that the probability of observing these  
410  $H_{D/A}$  values are less than one percent.

411 However, to examine a single hypothesis test of the null hypothesis, that the true  
412 Neandertal haplotype is not significantly longer than expected under neutrality, we  
413 performed a randomization test. First, we calculated mean  $H_{D/A}$  across this central  
414 locus (chr12:113344000-113450000). Next, we randomly chose one control SNP  
415 per true NLS (using the same matching conditions above) and calculated the mean  
416 of the control set. We repeated this procedure 100,000 times to create a normally

417 distributed null distribution, which we then used to calculate a Z-score (4.5) and  
418 corresponding P ( $3.35 \times 10^{-6}$ ) for our one-sided hypothesis test (Figure 2B).

419 Finally, we asked how unusual our observation of NLS frequency and  $H_{D/A}$  scores  
420 were across all simulations. Across approximately one million simulations  
421 (1,000,079), we only observed 413 simulations that produced an NLS with a  
422 frequency and  $H_{D/A}$  score as great or greater than the highest value observed  
423 among the true NLS (Figure 2C). In other words, the likelihood of our true sample  
424 under the neutral demographic scenario is less than  $5 \times 10^{-4}$ .

#### 425 *4. Analysis of ancient Eurasian data*

426 We utilized supplementary data table 3 from Mathieson et al. (2015). This table  
427 includes maximum likelihood allele frequency estimates for three ancient  
428 population samples (HG- Hunter-gatherer, EF- Early farmer, SA- Steppe ancestry)  
429 and four present day European samples from the 1,000 Genomes Project (see  
430 “Genome-wide scan for selection” section of methods in(Mathieson et al., 2015)).  
431 We intersect this table with allele frequencies for 1,000 Genomes Yorubans (YRI)  
432 and the Altai Neandertal genotypes and only analyze sites for which we have data  
433 for all samples (1,004,612 SNPs).

434 To calculate the expected allele frequency in modern samples under drift, we used  
435 the estimated proportions ( $m$ ) of (HG, EF, SA) in each of the four present-day  
436 samples estimated by Mathieson et al. (2015): CEU = (0.196, 0.257, 0.547), GBR

437 = (0.362, 0.229, 0.409), IBS = (0, 0.686, 0.314) and TSI = (0, 0.645, 0.355). We  
438 calculated the expected frequency  $E[p]$  of site as:

$$E[p] = \sum_{i \in \{HG, EF, SA\}} (p_i \times m_i)$$

439

440 Next, we calculated the absolute difference between observed and expected allele  
441 frequency in all four present-day European samples at all available sites. To test  
442 the null hypothesis that OAS NLS have not changed in frequency more than  
443 expected under neutrality at 11 SNPs in the central OAS region  
444 (chr12:113200000-113600000), we first calculated the fraction of all autosomal  
445 SNPs in the dataset at similar present-day frequency (within 1 percent in the  
446 folded frequency spectrum) of each OAS NLS. Finally, we calculated the fraction  
447 of autosomal SNPs with an absolute observed minus expected frequency  
448 difference greater than or equal to the OAS NLS. These results are given in Table  
449 1 and illustrated in Figure 2A.

450 This test does not explicitly incorporate variance in estimated ancient allele  
451 frequency. However, any bias in ancient allele frequency estimation should be  
452 distributed randomly across the genome. Therefore, our comparison to a genome-  
453 wide distribution of SNPs at similar present-day frequency should incorporate  
454 most of this error. Nonetheless, the selection test performed by Mathieson et  
455 al.(2015) does incorporate such error, so we can also look to the  $P_s$  from that test

456 to ensure consistency with our results. In fact, when considering OAS as a single  
457 locus, these results are highly significant and consistent with ours (see Table S1).

#### 458 *5. Estimation of selection coefficients*

459 To estimate the selection coefficient  $s$  under constant positive selection for a given  
460 starting frequency ( $x_0$ ), final frequency ( $x_1$ ), and number of generations between  
461 these estimates ( $\Delta t$ ), we assumed a model of standard logistic growth of a  
462 codominant allele:

$$463 \quad x_1 = x_0 / [x_0 + (1 - x_0) \exp(-s\Delta t)].$$

464 This equation can be easily solved to obtain  $s$ , given  $x_0$ ,  $x_1$ , and  $\Delta t$ .

#### 465 *6. Sample collection*

466 Buffy coats from 99 healthy European-descent donors were obtained from Indiana  
467 Blood Center (Indianapolis, IN, USA). Only individuals self-reported as currently  
468 healthy and not under medication were included in the study. The project was  
469 approved by the ethics committee at the CHU Sainte-Justine (protocol #4022). The  
470 individuals recruited in this study were males aged 18 to 55 years old.

#### 471 *7. DNA Extraction and genotyping*

472 DNA from each of the blood donors was extracted using the Gentra Pure Gene  
473 blood kit (Qiagen). Genotyping of each individual was then performed by  
474 Illumina's HumanOmni5Exome bead Chip array and complemented with imputed

475 data from the 1000 Genomes data using Impute2(Howie et al., 2009). Here, we  
476 only focused on genetic diversity surrounding the OAS region –  
477 chr12:113229549-113574044 (~ 344Kb) spanning from the beginning of *RPH3A*  
478 to the end of *RASAL1* – for a total of 673 SNPs with a MAF above 10%.

#### 479 *8. Isolation of monocytes and differentiation of macrophages*

480 Blood mononuclear cells were isolated by Ficoll-Paque centrifugation. Monocytes  
481 were purified from peripheral blood mononuclear cells (PBMCs) by positive  
482 selection with magnetic CD14 MicroBeads (Miltenyi Biotech) using the  
483 autoMACS Pro Separator. All samples had purity levels above 90%, as measured  
484 by flow cytometry using an antibody against CD14 (BD Biosciences). Monocytes  
485 were then cultured for 7 days in RPMI-1640 (Fisher) supplemented with 10%  
486 heat-inactivated FBS (FBS premium, US origin, Wisent), L-glutamine (Fisher)  
487 and M-CSF (20ng/mL; R&D systems). Cell cultures were fed every 2 days with  
488 complete medium supplemented with the cytokines previously mentioned. Before  
489 infection, we systematically verified that the differentiated macrophages presented  
490 the expected phenotype for non-activated macrophages (CD1a+, CD14+, CD83–,  
491 and HLA-DRlow (BD Biosciences)).

#### 492 *9. Bacterial preparation and infection of macrophages*

493 The day prior to infection, aliquots of *Salmonella typhimurium* (Keller strain) were  
494 thawed and bacteria were grown overnight in Tryptic Soy Broth (TSB) medium.  
495 Bacterial culture was diluted to mid-log phase prior to infection and supernatant

496 density was checked at OD600. Monocyte-derived macrophages were then  
497 infected with *Salmonella typhimurium* at a multiplicity of infection (MOI) of 10:1.  
498 A control group of non-infected macrophages was treated the same way but using  
499 medium without bacteria. After 2 hours in contact with the bacteria, macrophages  
500 were washed and cultured for another hour in the presence of 50 mg/ml of  
501 gentamycin in order to kill all extracellular bacteria present in the medium. The  
502 cells were then washed a second time and cultured in complete medium with 3  
503 mg/ml gentamycin for an additional 2 hours, the time point to which we refer in  
504 the main text.

#### 505 *10. Infection/stimulation of PBMC*

506 PBMCs from a subset of 30 individuals used to derive macrophages were cultured  
507 in RPMI-1640 (Fisher) supplemented with 10% heat-inactivated FBS (FBS  
508 premium, US origin, Wisent) and 1% L-glutamine (Fisher). The 30 individuals  
509 were chosen based on their genotype for kgp4570197, a SNP which derived allele  
510 is of Neandertal origin and that we used as a proxy to identify individuals  
511 harbouring the Neandertal haplotype in the OAS region. From the 30 individuals,  
512 and based on this SNP, 9 individuals were homozygous for the Neandertal  
513 haplotype, 9 were heterozygous, and 12 homozygous for the modern human  
514 sequence.

515 For each of the tested individuals, PBMCs (1 million per condition) were  
516 stimulated/infected with one of the following viral-associated immune challenges:  
517 polyI:C (10 µg/ml, TLR3 agonist), gardiquimod (0.5µg/ml, TLR7 and TLR8



518 agonist), Influenza PR8 WT (multiplicity of infection (MOI) of 0.05:1), Herpes  
519 simplex virus (HSV) 1 ( $1.55 \times 10^2$  CPE), and HSV2 ( $19.5 \times 10^4$  CPE). PBMCs were  
520 stimulated/infected for 4 hours with TLR ligands and Influenza, and 6h with  
521 HSV1 and HSV2. A control group of non-infected PBMC was treated the same  
522 way but with only medium.

### 523 *11. RNA extraction, RNA-seq library preparation, and sequencing*

524 Total RNA was extracted from the non-infected and infected/stimulated cells  
525 using the miRNeasy kit (Qiagen). RNA quantity was evaluated  
526 spectrophotometrically, and the quality was assessed with the Agilent 2100  
527 Bioanalyzer (Agilent Technologies). Only samples with no evidence of RNA  
528 degradation (RNA integrity number > 8) were kept for further experiments. RNA-  
529 sequencing libraries were prepared using the Illumina TruSeq protocol. Once  
530 prepared, indexed cDNA libraries were pooled (6 libraries per pool) in equimolar  
531 amounts and sequenced with single-end 100bp reads on an Illumina HiSeq2500.  
532 Results based on the entire dataset are described elsewhere (Nédélec *et al.*, under  
533 revision). Here, we only studied transcript-level and gene-level expression  
534 estimates for *OAS1*, *OAS2* and *OAS3*.

### 535 *12. Quantifying gene expression values from RNA-seq data*

536 Adaptor sequences and low quality score bases (Phred score < 20) were first  
537 trimmed using Trim Galore (version 0.2.7). The resulting reads were then mapped  
538 to the human genome reference sequence (Ensembl GRCh37 release 65) using

539 TopHat (version 2.0.6) and using a hg19 transcript annotation database  
540 downloaded from UCSC. Gene-level expression estimates were calculated using  
541 featureCounts (version 1.4.6-p3) and transcript-level expression values were  
542 obtained using RSEM under default parameters.

### 543 *13. Quantitative real time PCR*

544 For the PBMC samples we measured the expression levels of OAS and interferon  
545 genes using real time PCR. 100ng of high-quality RNA was reverse-transcribed  
546 into cDNA using the qScript cDNA SuperMix (Quanta Biosciences). Quantitative  
547 real time PCR was performed using 96.96 Dynamic Array™ IFCs and the  
548 BioMark™ HD System from Fluidigm. For the TaqMan gene assays, we used the  
549 following TaqMan Gene Expression Assay (Applied BioSystems) to quantify the  
550 expression levels of interferon genes: *IFNA1* (Hs03044218), *IFNA6*  
551 (Hs00819627), and *IFNG* (Hs00989291). To quantify the overall expression levels  
552 of OAS genes, we used probes that capture all common isoforms of *OAS1*  
553 (Hs00973635), *OAS2* (Hs00942643), and *OAS3* (Hs00196324). Custom-made  
554 probes were designed to specifically target the short-isoform of *OAS2* (Forward  
555 Primer Sequence CTGCAGGAACCCGAACAGTT; Reverse Primer Sequence  
556 ACTCATGGCCTAGAGGTTGCA; Reporter Sequence  
557 AGAGAAAAGCCAAAGAA). As housekeeping genes we used: *GAPDH*  
558 (Hs02758991), *GUSB* (Hs99999908), *HPRT1* (Hs99999909), and *POLR2A*  
559 (Hs00172187). The results reported in the manuscript used *POLR2A* as a reference  
560 but all conclusions remain unchanged when using any of the other housekeeping  
561 genes.

562 We start by doing a preamplification of the cDNA using the PreAmp Master Mix  
563 (Fluidigm). Preamplified cDNA was then diluted 2X on a solution of 10 mM Tris–  
564 HCl (pH 8.0) and 0.1 mM EDTA. In order to prepare samples for loading into the  
565 integrated fluid circuit (IFC), a mix was prepared consisting of 360  $\mu$ L TaqMan  
566 Fast Advanced Master Mix (Applied BioSystems) and 36  $\mu$ L 20 $\times$  GE Sample  
567 Loading Reagent (Fluidigm). 2.75  $\mu$ L of this mix was dispensed to each well of a  
568 96-well assay plate and mixed with 2.25  $\mu$ L of preamplified cDNA. Following  
569 priming of the IFC in the IFC Controller HX, 5  $\mu$ L of the mixture of cDNA and  
570 loading reagent were dispensed in each of the sample inlet of the 96.96 IFC. For  
571 the TaqMan gene assays, 5  $\mu$ L of mixes consisting of 2.5  $\mu$ L 20 $\times$  TaqMan Gene  
572 Expression Assay (Applied BioSystems) and 2.5  $\mu$ L 2X Assay Loading Reagent  
573 (Fluidigm) were dispensed to each detector inlet of the 96.96 IFC. After loading  
574 the assays and samples into the IFC in the IFC Controller HX, the IFC was  
575 transferred to the BioMark HD and PCR was performed using the thermal protocol  
576 GE 96  $\times$  96 Fast v1.pcl. This protocol consists of a Thermal Mix of 70  $^{\circ}$ C, 30 min;  
577 25  $^{\circ}$ C, 10 min, Hot Start at 95  $^{\circ}$ C, 1 min, PCR Cycle of 35 cycles of (96  $^{\circ}$ C, 5 s;  
578 60  $^{\circ}$ C, 20 s). Data was analysed using Fluidigm Real-Time PCR Analysis software  
579 using the Linear (Derivative) Baseline Correction Method and the Auto  
580 (Detectors) Ct Threshold Method.

581 To quantify the expression levels of the *OAS1* isoform associated with the derived  
582 allele at the splicing variant rs10774671 we used SybrGreen and the following  
583 forward (GCTGAGGCCTGGCTGAATTA), and reverse  
584 (CCACTTGTTAGCTGATGTCCTTGA) primers. PCR was performed using the

585 thermal protocol 50 °C, 2 min; 95 °C, 10 min, PCR Cycle of 40 cycles of (95 °C,  
586 15 s; 60 °C, 1 min). A melting curve was also performed to check for non-specific  
587 amplification.

#### 588 *14. Genotype–Phenotype Association Analysis*

589 eQTL, asQTL were performed against *OAS1*, *OAS2* and *OAS3*. We examined  
590 associations between SNP genotypes and the phenotype of interest using a linear  
591 regression model, in which phenotype was regressed against genotype. In  
592 particular, expression levels were considered as the phenotype when searching for  
593 eQTL and the percentage usage of each isoform in each gene when mapping  
594 asQTL. To avoid low power caused by rare variants, only SNPs in the OAS region  
595 with a minor allele frequency of 10% across all individuals were tested (i.e., 673  
596 SNPs within the region chr12:113229549-113574044). In all cases, we assumed  
597 that alleles affected the phenotype in an additive manner. For the eQTL and  
598 asQTL analyses on macrophages we mapped Salmonella-infected, and non-  
599 infected samples separately. For the non-infected and infected/stimulated PBMCs  
600 we only tested expression levels against the SNPs identified as eQTL or asQTL in  
601 the macrophage data (specifically, the SNPs for which boxplots are shown in  
602 Figure 3).

603 **Author Contributions:** Conception and design: AJS, PWM, LBB; Acquisition of  
604 data: AJS, AD, YN, VY, LBB; Analysis and interpretation of data: AJS, AD, YN,  
605 PWM, LBB; Contributed unpublished, essential data, or reagents: CA, JET;  
606 Drafting or revising the article: AJS, PWM, LBB.

607

608 **Acknowledgements:** We thank all members from the Barreiro and Messer lab for  
609 helpful discussions and comments on the manuscript. We thank Dr Silvia Vidal for  
610 the gift of the Influenza PR8 WT used in this study, Dr Hugo Soudeyins and Doris  
611 Ransy for advice with the viral infections, and Marc Montero and George (PJ)  
612 Perry for sharing their analysis on nucleotide diversity levels of OAS genes in  
613 non-human primate species.

614

615 **Funding Statement:** This study was funded by grants from the Canadian  
616 Institutes of Health Research (301538 and 232519), the Human Frontiers Science  
617 Program (CDA-00025/2012) and the Canada Research Chairs Program (950-  
618 228993) (to L.B.B.). Y.N. was supported by a fellowship from the *Réseau de*  
619 *Médecine Génétique Appliquée* (RMGA).

620 **References:**

621 Awady, El, M.K., Anany, M.A., Esmat, G., Zayed, N., Tabll, A.A., Helmy, A.,  
622 Zayady, El, A.R., Abdalla, M.S., Sharada, H.M., Raziky, El, M., Akel, El, W.,  
623 Abdalla, S., Bader El Din, N.G., 2011. Single nucleotide polymorphism at  
624 exon 7 splice acceptor site of OAS1 gene determines response of hepatitis C  
625 virus patients to interferon therapy. *Journal of Gastroenterology and*  
626 *Hepatology*. 26, 843–850.  
627 Bigham, A.W., Buckingham, K.J., Husain, S., Emond, M.J., Bofferding, K.M.,  
628 Gildersleeve, H., Rutherford, A., Astakhova, N.M., Perelygin, A.A., Busch,  
629 M.P., Murray, K.O., Sejvar, J.J., Green, S., Kriesel, J., Brinton, M.A.,  
630 Bamshad, M., 2011. Host Genetic Risk Factors for West Nile Virus Infection  
631 and Disease Progression. *PLoS ONE*. 6, e24745.  
632 Bonnevie-Nielsen, V., Field, L.L., Lu, S., Zheng, D.-J., Li, M., Martensen, P.M.,  
633 Nielsen, T.B., Beck-Nielsen, H., Lau, Y.L., Pociot, F., 2005. Variation in  
634 antiviral 2',5'-oligoadenylate synthetase (2"5"AS) enzyme activity is  
635 controlled by a single-nucleotide polymorphism at a splice-acceptor site in the  
636 OAS1 gene. *The American Journal of Human Genetics*. 76, 623–633.  
637 Chen, G.K., Marjoram, P., Wall, J.D., 2009. Fast and flexible simulation of DNA

- 638 sequence data. *Genome Research*. 19, 136–142.
- 639 Consortium, T.I.G.P., 2015. A global reference for human genetic variation.
- 640 *Nature*. 526, 68–74.
- 641 Deschamps, M., Laval, G., Fagny, M., Itan, Y., Abel, L., Casanova, J.-L., Patin,
- 642 E., Quintana-Murci, L., 2016. Genomic Signatures of Selective Pressures and
- 643 Introgression from Archaic Hominins at Human Innate Immunity Genes.
- 644 *American Journal of Human Genetics*. 98, 5–21.
- 645 Ferrer-Admetlla, A., Liang, M., Korneliussen, T., Nielsen, R., 2014. On detecting
- 646 incomplete soft or hard selective sweeps using haplotype structure. *Molecular*
- 647 *Biology and Evolution*. 31, 1275–1291.
- 648 Fu, Q., Li, H., Moorjani, P., Jay, F., Slepchenko, S.M., Bondarev, A.A., Johnson,
- 649 P.L.F., Aximu-Petri, A., Prüfer, K., de Filippo, C., Meyer, M., Zwyns, N.,
- 650 Salazar-García, D.C., Kuzmin, Y.V., Keates, S.G., Kosintsev, P.A., Razhev,
- 651 D.I., Richards, M.P., Peristov, N.V., Lachmann, M., Douka, K., Higham,
- 652 T.F.G., Slatkin, M., Hublin, J.-J., Reich, D., Kelso, J., Viola, T.B., Pääbo, S.,
- 653 2014. Genome sequence of a 45,000-year-old modern human from western
- 654 Siberia. *Nature*. 514, 445–449.
- 655 Gravel, S., Henn, B.M., Gutenkunst, R.N., Indap, A.R., Marth, G.T., Clark, A.G.,
- 656 Yu, F., Gibbs, R.A., Bustamante, C.D., Project, 1.G., 2011. Demographic
- 657 history and rare allele sharing among human populations. *Proceedings of the*
- 658 *National Academy of Sciences of the United States of America*. 108, 11983–
- 659 11988.
- 660 Green, R.E., Krause, J., Briggs, A.W., Maricic, T., Stenzel, U., Kircher, M.,
- 661 Patterson, N., Li, H., Zhai, W., Fritz, M.H.-Y., 2010. A draft sequence of the
- 662 Neandertal genome. *Science*. 328, 710–722.
- 663 Gulig, P.A., Doyle, T.J., Clare-Salzler, M.J., Maiese, R.L., Matsui, H., 1997.
- 664 Systemic infection of mice by wild-type but not Spv- *Salmonella typhimurium*
- 665 is enhanced by neutralization of gamma interferon and tumor necrosis factor
- 666 alpha. *Infection and Immunity*. 65, 5191–5197.
- 667 Howie, B.N., Donnelly, P., Marchini, J., 2009. A Flexible and Accurate Genotype
- 668 Imputation Method for the Next Generation of Genome-Wide Association
- 669 Studies. *PLoS Genetics*. 5, e1000529.
- 670 Hublin, J.J., 2009. The origin of Neandertals. *Proceedings of the National*
- 671 *Academy of Sciences*. 106, 16022–16027.
- 672 Kent, W.J., Sugnet, C.W., Furey, T.S., Roskin, K.M., Pringle, T.H., Zahler, A.M.,
- 673 Haussler, D., 2002. The human genome browser at UCSC. *Genome Research*.
- 674 12, 996–1006.
- 675 Kwon, Y.-C., Kang, J.-I., Hwang, S.B., Ahn, B.-Y., 2012. The ribonuclease I-
- 676 dependent antiviral roles of human 2',5'-oligoadenylate synthetase family
- 677 members against hepatitis C virus. *FEBS letters*. 587, 156–164.
- 678 LaRock, D.L., Chaudhary, A., Miller, S.I., 2015. *Salmonellae* interactions with
- 679 host processes. *Nature Reviews Microbiology*. 13, 191–205.
- 680 Lazaridis, I., Patterson, N., Mittnik, A., Renaud, G., Mallick, S., Kirsanow, K.,
- 681 Sudmant, P.H., Schraiber, J.G., Castellano, S., Lipson, M., Berger, B.,
- 682 Economou, C., Bollongino, R., Fu, Q., Bos, K.I., Nordenfelt, S., Li, H., de
- 683 Filippo, C., Prüfer, K., Sawyer, S., Posth, C., Haak, W., Hallgren, F.,

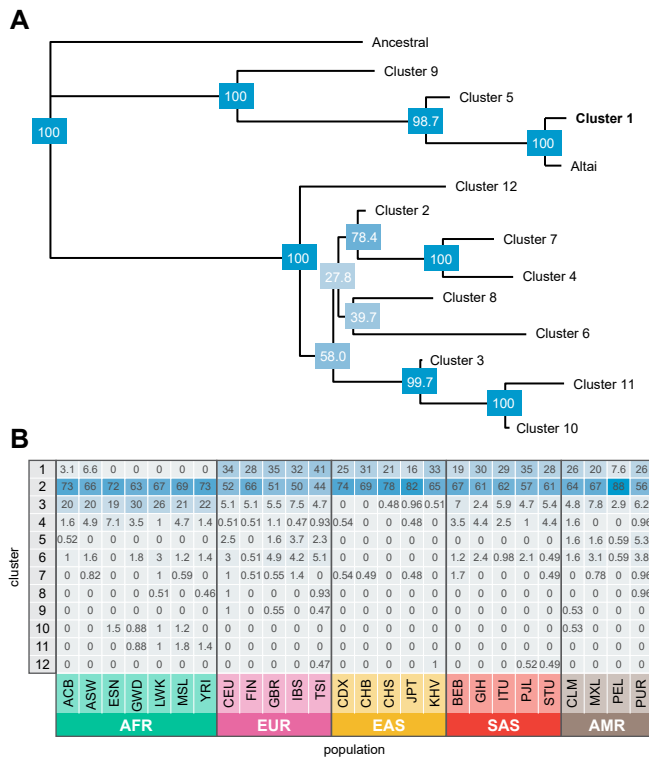
- 684 Fornander, E., Rohland, N., Delsate, D., Francken, M., Guinet, J.-M., Wahl, J.,  
685 Ayodo, G., Babiker, H.A., Bailliet, G., Balanovska, E., Balanovsky, O.,  
686 Barrantes, R., Bedoya, G., Ben-Ami, H., Bene, J., Berrada, F., Bravi, C.M.,  
687 Brisighelli, F., Busby, G.B.J., Cali, F., Churnosov, M., Cole, D.E.C., Corach,  
688 D., Damba, L., van Driem, G., Dryomov, S., Dugoujon, J.-M., Fedorova, S.A.,  
689 Romero, I.G., Gubina, M., Hammer, M., Henn, B.M., Hervig, T., Hodoglugil,  
690 U., Jha, A.R., Karachanak-Yankova, S., Khusainova, R., Khusnutdinova, E.,  
691 Kittles, R., Kivisild, T., Klitz, W., Kucinskis, V., Kushniarevich, A., Laredj,  
692 L., Litvinov, S., Loukidis, T., Mahley, R.W., Melegh, B., Metspalu, E.,  
693 Molina, J., Mountain, J., Näkkäläjärvi, K., Nesheva, D., Nyambo, T., Osipova,  
694 L., Parik, J., Platonov, F., Posukh, O., Romano, V., Rothhammer, F., Rudan,  
695 I., Ruizbakiev, R., Sahakyan, H., Sajantila, A., Salas, A., Starikovskaya, E.B.,  
696 Tarekegn, A., Toncheva, D., Turdikulova, S., Uktveryte, I., Utevska, O.,  
697 Vasquez, R., Villena, M., Voevoda, M., Winkler, C.A., Yepiskoposyan, L.,  
698 Zalloua, P., Zemunik, T., Cooper, A., Capelli, C., Thomas, M.G., Ruiz-  
699 Linares, A., Tishkoff, S.A., Singh, L., Thangaraj, K., Villems, R., Comas, D.,  
700 Sukernik, R., Metspalu, M., Meyer, M., Eichler, E.E., Burger, J., Slatkin, M.,  
701 Pääbo, S., Kelso, J., Reich, D., Krause, J., 2014. Ancient human genomes  
702 suggest three ancestral populations for present-day Europeans. *Nature*. 513,  
703 409–413.
- 704 Lim, J.K., Lisco, A., McDermott, D.H., Huynh, L., Ward, J.M., Johnson, B.,  
705 Johnson, H., Pape, J., Foster, G.A., Krysztof, D., Follmann, D., Stramer, S.L.,  
706 Margolis, L.B., Murphy, P.M., 2009. Genetic Variation in OAS1 Is a Risk  
707 Factor for Initial Infection with West Nile Virus in Man. *PLoS Pathogens*. 5,  
708 e1000321.
- 709 Llorente, M.G., Jones, E.R., Eriksson, A., Siska, V., Arthur, K.W., Arthur, J.W.,  
710 Curtis, M.C., Stock, J.T., Coltorti, M., Pieruccini, P., Stretton, S., Brock, F.,  
711 Higham, T., Park, Y., Hofreiter, M., G, B.D., Bhak, J., Pinhasi, R., Manica,  
712 A., 2015. Ancient Ethiopian genome reveals extensive Eurasian admixture  
713 throughout the African continent. *Science*.
- 714 Mathieson, I., Lazaridis, I., Rohland, N., Mallick, S., Patterson, N., Roodenberg,  
715 S.A., Harney, E., Stewardson, K., Fernandes, D., Novak, M., Sirak, K.,  
716 Gamba, C., Jones, E.R., Llamas, B., Dryomov, S., Pickrell, J., Arsuaga, J.L.,  
717 de Castro, J.M.B., Carbonell, E., Gerritsen, F., Khokhlov, A., Kuznetsov, P.,  
718 Lozano, M., Meller, H., Mochalov, O., Moiseyev, V., Guerra, M.A.R.,  
719 Roodenberg, J., Vergès, J.M., Krause, J., Cooper, A., Alt, K.W., Brown, D.,  
720 Anthony, D., Lalueza-Fox, C., Haak, W., Pinhasi, R., Reich, D., 2015.  
721 Genome-wide patterns of selection in 230 ancient Eurasians. *Nature*.
- 722 Mendez, F.L., Watkins, J.C., Hammer, M.F., 2012. A Haplotype at STAT2  
723 Introgressed from Neanderthals and Serves as a Candidate of Positive  
724 Selection in Papua New Guinea. *The American Journal of Human Genetics*.  
725 91, 265–274.
- 726 Mendez, F.L., Watkins, J.C., Hammer, M.F., 2013. Neandertal origin of genetic  
727 variation at the cluster of OAS immunity genes. *Molecular Biology and*  
728 *Evolution*. 30, 798–801.
- 729 Meyer, M., Arsuaga, J.L., de Filippo, C., Nagel, S., Aximu-Petri, A., Nickel, B.,

- 730 Martínez, I., Gracia, A., de Castro, J.M.B., Carbonell, E., Viola, B., Kelso, J.,  
731 Prüfer, K., Pääbo, S., 2016. Nuclear DNA sequences from the Middle  
732 Pleistocene Sima de los Huesos hominins. *Nature*.
- 733 Meyer, M., Kircher, M., Gansauge, M.T., Li, H., Racimo, F., Mallick, S.,  
734 Schraiber, J.G., Jay, F., Prüfer, K., de Filippo, C., 2012. A high-coverage  
735 genome sequence from an archaic denisovan individual. *Science*. 338, 222–  
736 226.
- 737 Nauciel, C., Espinasse-Maes, F., 1992. Role of Gamma Interferon and Tumor-  
738 Necrosis-Factor-Alpha in Resistance to Salmonella-Typhimurium Infection.  
739 *Infection and Immunity*. 60, 450–454.
- 740 Player, M.R., Torrence, P.F., 1998. The 2–5 A system: Modulation of viral and  
741 cellular processes through acceleration of RNA degradation. *Pharmacology &*  
742 *Therapeutics*. 78, 55–113.
- 743 Prüfer, K., Racimo, F., Patterson, N., Jay, F., Sankararaman, S., Sawyer, S.,  
744 Heinze, A., Renaud, G., Sudmant, P.H., de Filippo, C., Li, H., Mallick, S.,  
745 Dannemann, M., Fu, Q., Kircher, M., Kuhlwilm, M., Lachmann, M., Meyer,  
746 M., Ongyerth, M., Siebauer, M., Theunert, C., Tandon, A., Moorjani, P.,  
747 Pickrell, J., Mullikin, J.C., Vohr, S.H., Green, R.E., Hellmann, I., Johnson,  
748 P.L.F., Blanche, H., Cann, H., Kitzman, J.O., Shendure, J., Eichler, E.E., Lein,  
749 E.S., Bakken, T.E., Golovanova, L.V., Doronichev, V.B., Shunkov, M.V.,  
750 Derevianko, A.P., Viola, B., Slatkin, M., Reich, D., Kelso, J., Pääbo, S., 2014.  
751 The complete genome sequence of a Neanderthal from the Altai Mountains.  
752 *Nature*. 505, 43–49.
- 753 Racimo, F., Marnetto, D., Huerta-Sanchez, E., 2016. The landscape of uniquely  
754 shared archaic alleles in present-day human populations. *bioRxiv*. 045237.
- 755 Racimo, F., Sankararaman, S., Nielsen, R., Huerta-Sanchez, E., 2015. Evidence  
756 for archaic adaptive introgression in humans. *Nature Reviews Genetics*.
- 757 Reich, D., Green, R.E., Kircher, M., Krause, J., Patterson, N., Durand, E.Y., Viola,  
758 B., Briggs, A.W., Stenzel, U., Johnson, P.L.F., 2010. Genetic history of an  
759 archaic hominin group from Denisova Cave in Siberia. *Nature*. 468, 1053–  
760 1060.
- 761 Sabeti, P.C., Reich, D.E., Higgins, J.M., Levine, H.Z.P., Richter, D.J., Schaffner,  
762 S.F., Gabriel, S.B., Platko, J.V., Patterson, N.J., McDonald, G.J., 2002.  
763 Detecting recent positive selection in the human genome from haplotype  
764 structure. *Nature*. 419, 832–837.
- 765 Sankararaman, S., Mallick, S., Dannemann, M., Prüfer, K., Kelso, J., Pääbo, S.,  
766 Patterson, N., Reich, D., 2014. The genomic landscape of Neanderthal  
767 ancestry in present-day humans. *Nature*. 507, 354–357.
- 768 Sankararaman, S., Mallick, S., Patterson, N., Reich, D., 2016. The Combined  
769 Landscape of Denisovan and Neanderthal Ancestry in Present-Day Humans.  
770 *Current Biology*.
- 771 Sawyer, S., Renaud, G., Viola, B., Hublin, J.-J., Gansauge, M.-T., Shunkov, M.V.,  
772 Derevianko, A.P., Prüfer, K., Kelso, J., Pääbo, S., 2015. Nuclear and  
773 mitochondrial DNA sequences from two Denisovan individuals. *Proceedings*  
774 *of the National Academy of Sciences*. 201519905.
- 775 Schlamp, F., Made, J., Stambler, R., Chesebrough, L., Boyko, A.R., Messer, P.W.,



776           2016. Evaluating the performance of selection scans to detect selective sweeps  
777           in domestic dogs. *Molecular Ecology*. 25, 342–356.  
778       Ségurel, L., Quintana-Murci, L., 2014. Preserving immune diversity through  
779           ancient inheritance and admixture. *Current opinion in immunology*. 30C, 79–  
780           84.  
781       Tennessen, J.A., Bigham, A.W., O'Connor, T.D., Fu, W., Kenny, E.E., Gravel, S.,  
782           McGee, S., Do, R., Liu, X., Jun, G., Kang, H.M., Jordan, D., Leal, S.M.,  
783           Gabriel, S., Rieder, M.J., Abecasis, G., Altshuler, D., Nickerson, D.A.,  
784           Boerwinkle, E., Sunyaev, S., Bustamante, C.D., Bamshad, M.J., Akey, J.M.,  
785           Broad GO, Seattle GO, on behalf of the NHLBI Exome Sequencing Project,  
786           2012. Evolution and Functional Impact of Rare Coding Variation from Deep  
787           Sequencing of Human Exomes. *Science*. 337, 64–69.  
788       Vernot, B., Akey, J.M., 2014. Resurrecting surviving Neandertal lineages from  
789           modern human genomes. *Science*. 343, 1021.  
790       Vernot, B., Akey, J.M., 2015. Complex History of Admixture between Modern  
791           Humans and Neandertals. *The American Journal of Human Genetics*.  
792       Voight, B.F., Kudravalli, S., Wen, X., Pritchard, J.K., 2006. A map of recent  
793           positive selection in the human genome. *PLoS Biology*. 4, e72.  
794       Yang, M.A., Malaspinas, A.S., Durand, E.Y., Slatkin, M., 2012. Ancient structure  
795           in Africa unlikely to explain Neanderthal and non-African genetic similarity.  
796           *Molecular Biology and Evolution*. 29, 2987–2995.  
797  
798  
799  
800  
801  
802  
803

804



805

806

807 Figure 1: Neandertal introgressed haplotypes in the OAS region. (A) Neighbor-

808 joining tree of 5008 phased haplotypes spanning chr12: 113344739-113449528

809 (hg19) from phase 3 of the 1000 genomes project. Haplotypes condensed into 12

810 core haplotypes based on majority allele in clusters with pairwise differences of 85

811 or less. The figure illustrates that the Altai haplotype is very similar to “cluster 1”

812 haplotypes found in several human populations. Bootstrap values (1000 replicates)

813 are provided in blue boxes at each node. (B) Frequencies of the 12 core haplotypes

814 within each 1000 genomes project population sample. The most common

815 Neandertal-like haplotype, cluster 1, is found only outside of sub-Saharan African

816 samples, with the exception of recently admixed populations. Population codes

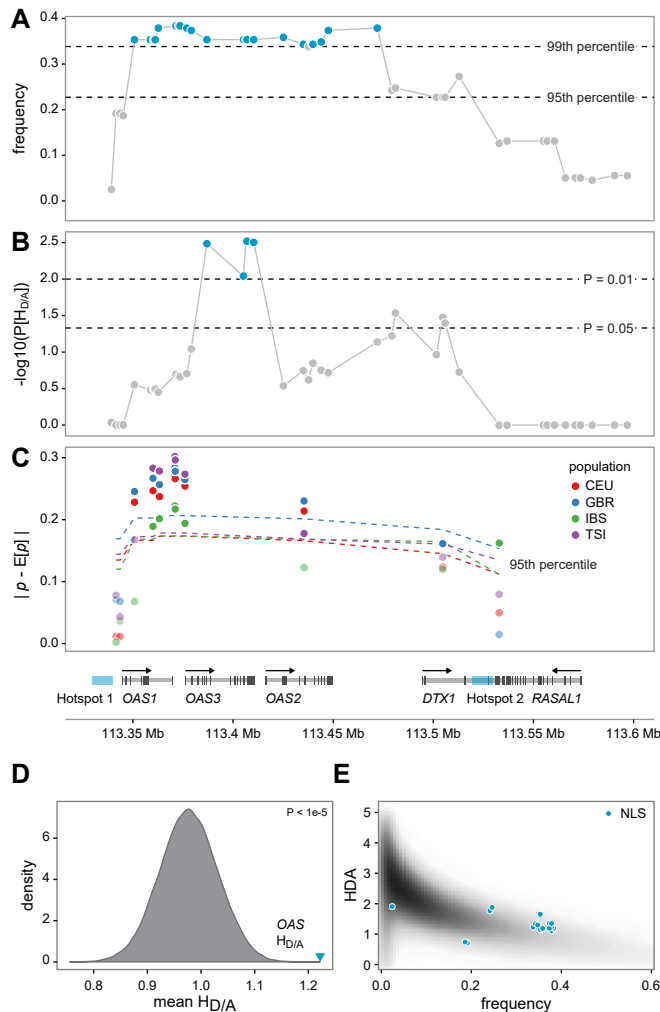
817 can be found at <http://www.1000genomes.org/category/population/>.

818

819

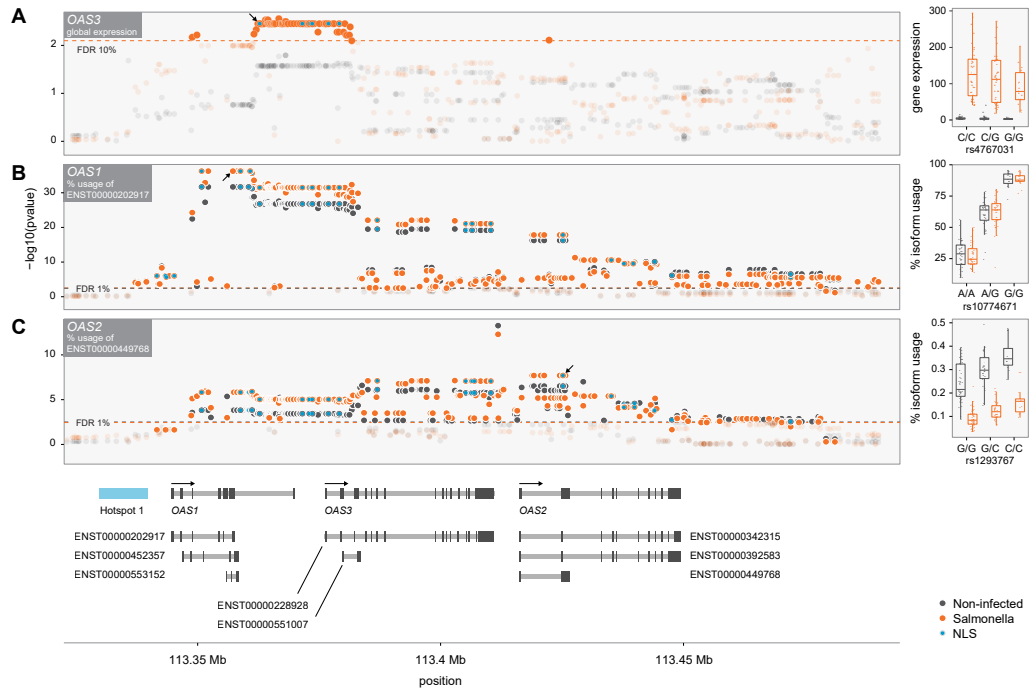
820

821



822  
823

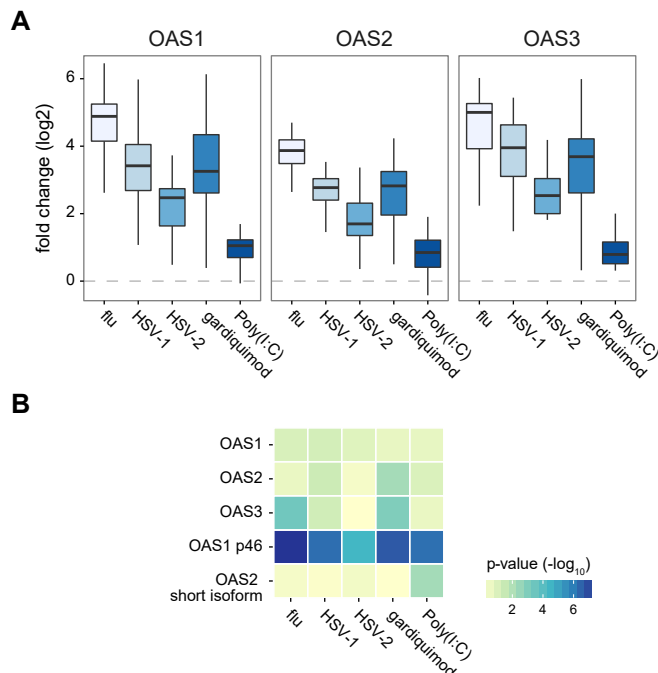
824 Figure 2: OAS-introgressed haplotypes show multiple signatures of positive  
825 selection. (A) Comparison of frequency (y-axis) of NLS in the OAS locus in CEU  
826 sample with respect to neutral expectations (dashed lines) based on coalescent  
827 simulations. (B) The  $H_{D/A}$  values associated with several NLS are significantly  
828 larger ( $-\log_{10} P_s$  in the y-axis) than expected under a neutral model of evolution.  
829  $H_{D/A}$  at each NLS in the OAS region were compared against the distributions of  
830 simulated NLS drawn to match local recombination rate and allele frequency. (C)  
831 Absolute difference between observed and expected allele frequency in all four  
832 present-day European samples (y-axis) based on ancient DNA data. Dashed lines  
833 represent the 95<sup>th</sup> percentile of the expected distribution based on similar  
834 deviations calculated on a dataset of approximately one million SNPs scattered  
835 around the genome and with comparable present-day frequencies to those found  
836 for NLS in the OAS region (D) Comparison of mean  $H_{D/A}$  across OAS locus to  
837 randomized frequency and genomic position-matched SNPs from simulations.  
838 OAS locus is a strong outlier ( $p < 10^{-5}$ ) compared to simulations. (E) Joint density  
839 distribution of  $H_{D/A}$  and Neandertal-like site derived frequency. Cluster of NLS in  
840 OAS are significant outliers to neutral distribution ( $p < 5 \times 10^{-4}$ ).



841  
842  
843  
844  
845  
846  
847  
848  
849  
850  
851  
852  
853  
854  
855  
856  
857  
858  
859  
860  
861  
862  
863  
864  
865  
866  
867

Figure 3: Pervasive impact of the Neandertal haplotype on the regulation of *OAS* genes in primary macrophages. (A)  $-\log_{10} P$ s (y-axis) for the association between genotypes for SNPs with a MAF > 10% in the OAS region and expression levels of *OAS3* in non-infected (black) and *Salmonella*-infected macrophages (orange). The dashed line shows the P cutoff corresponding to an FDR of 10%. The right panel shows a boxplot for the association between genotypes at the NLS rs4767031 (x-axis) and the expression levels of *OAS3* (y-axis). (B)  $-\log_{10} P$ s (y-axis) for the association between genotypes in the OAS regions and the percentage usage of isoform ENST00000202917 (i.e., p46 in the text) in non-infected (black) and *Salmonella*-infected macrophages (orange). The dashed line shows the P cutoff corresponding to an FDR of 1%. The right panel shows a boxplot for the association between genotypes at the splicing variant rs10774671 (x-axis) and the percentage usage of isoform p46 (y-axis). (C) Similar to (B) but for the percentage usage of isoform ENST00000449768 of *OAS2*. In all the panels NLS are highlighted by blue dots. The arrows on panel A-C highlight the location of the SNPs for which the boxplots are shown on the right.

868



869

870

871

872

873 Figure 4: The Neandertal haplotype in the OAS regions has a different impact on

874 the regulation of OAS genes depending on the viral agents PBMCs are exposed to.

875 (A) Log<sub>2</sub> fold induction (y-axis) of *OAS1*, *OAS2* and *OAS3* in response to

876 different viral agents or viral-associated immune stimuli (B)  $-\log_{10} P$  for the

877 association between genotype status for the Neandertal haplotype and overall

878 expression levels of OAS genes and the expression of specific isoforms of *OAS1*

879 and *OAS2* (those identified in Figure 3 as associated with NLS).

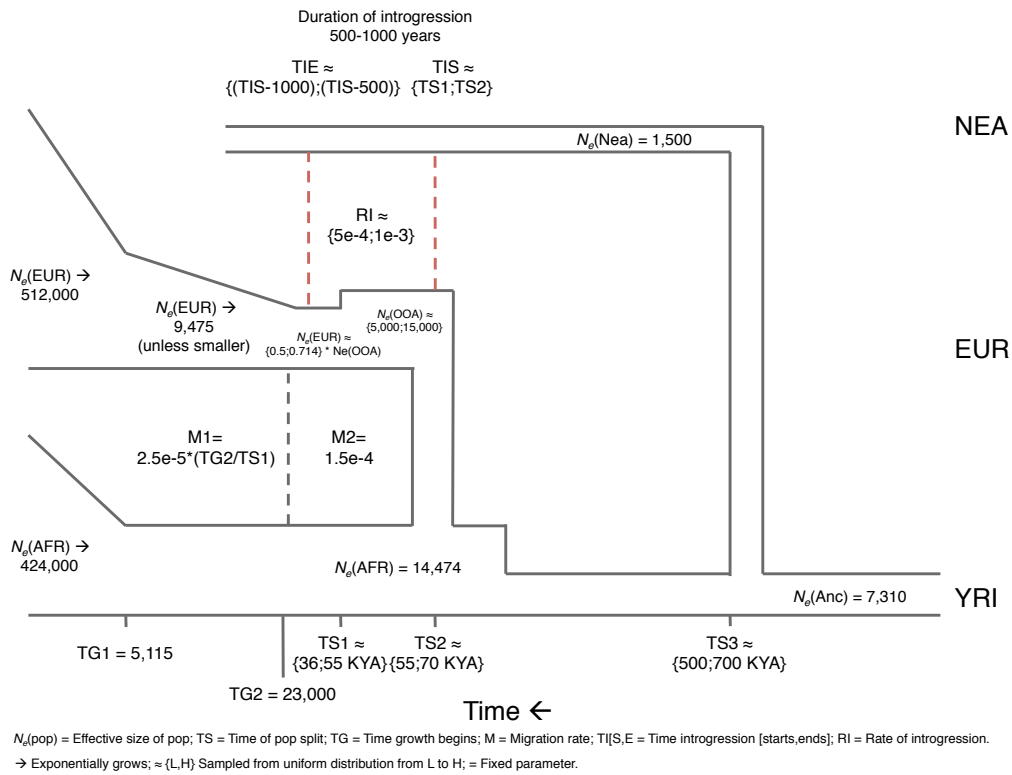
880

881

882

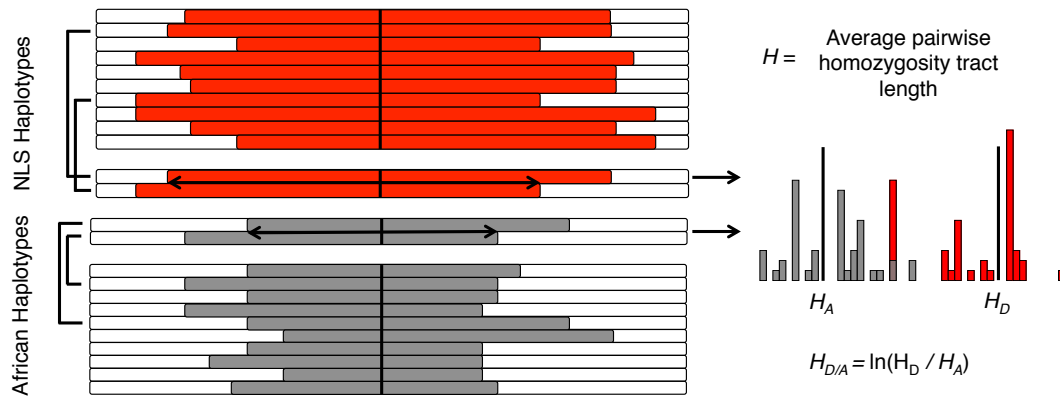
883  
884  
885

Supplementary Figures:



886  
887  
888  
889  
890  
891  
892  
893  
894  
895

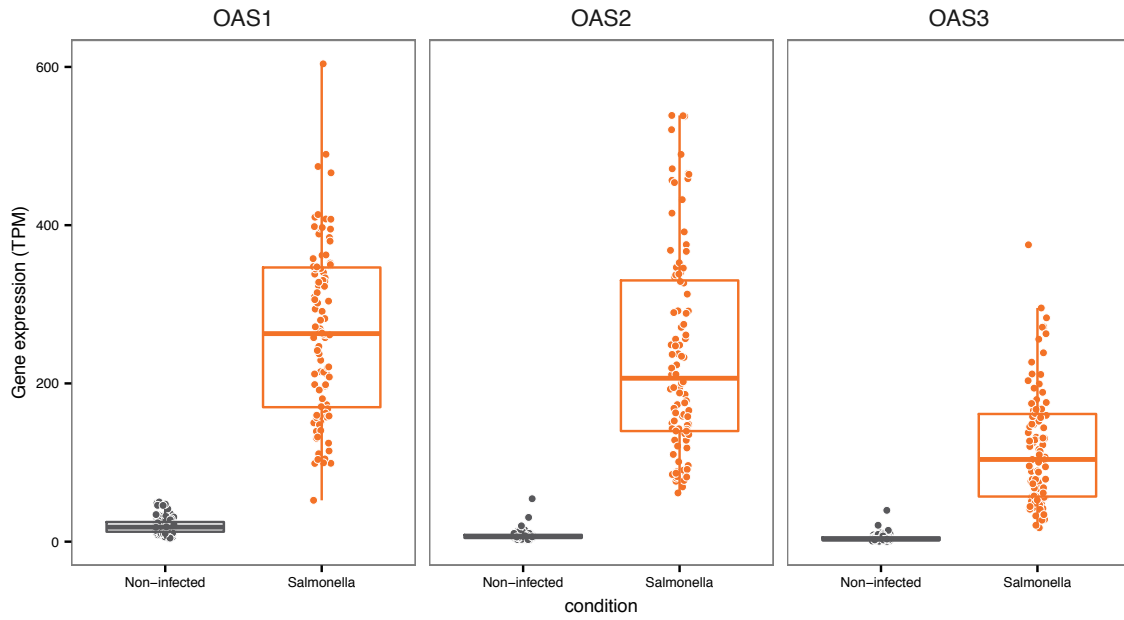
Supplementary Figure 1: Demographic model for neutral coalescent simulations.



896  
 897  
 898  
 899  
 900  
 901

Supplementary Figure 2: Illustration of  $H_{D/A}$  statistic.

902  
903

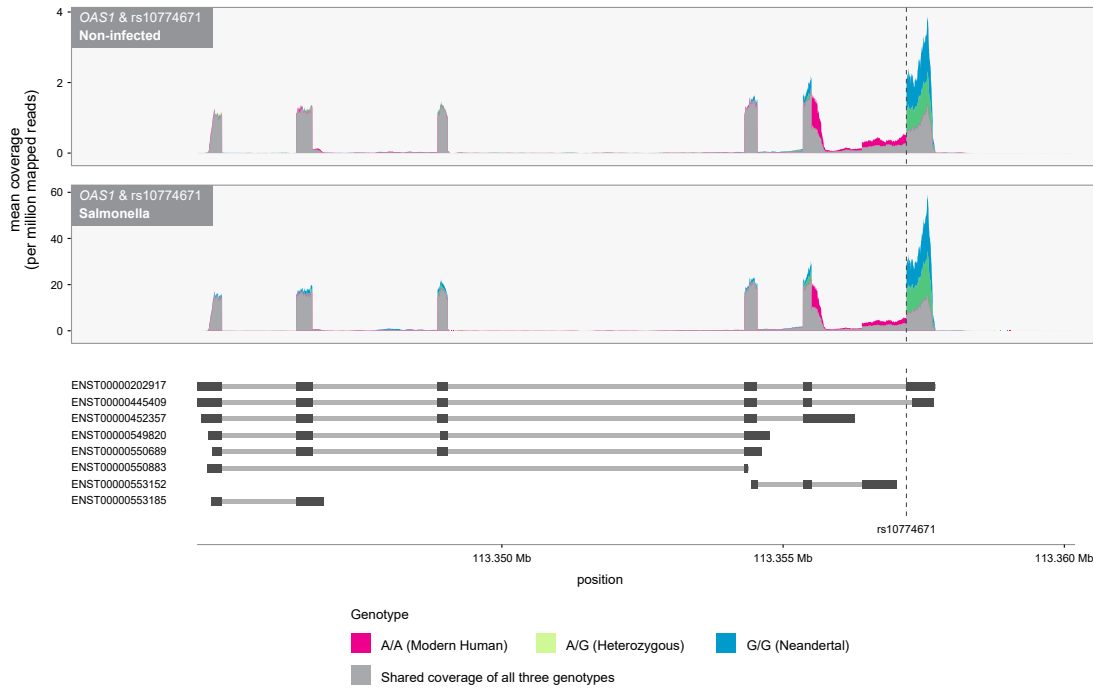


904  
905  
906  
907  
908  
909

Supplementary Figure 3: Expression levels of OAS genes in primary macrophages before and after infection with *Salmonella*.



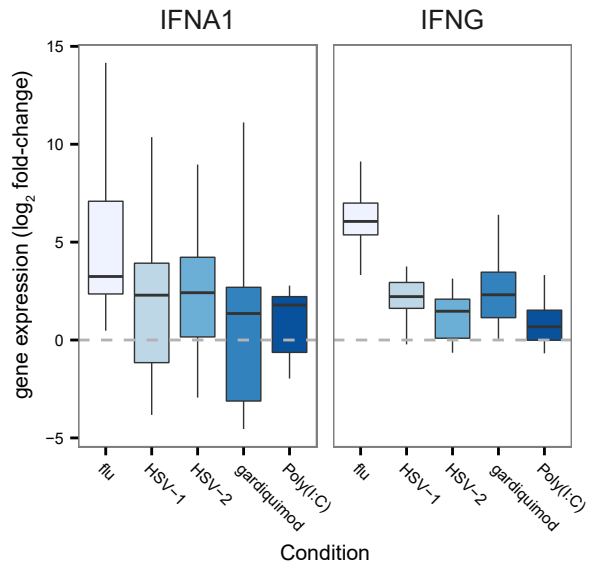
910  
911



912  
913  
914  
915  
916  
917  
918  
919  
920  
921  
922  
923

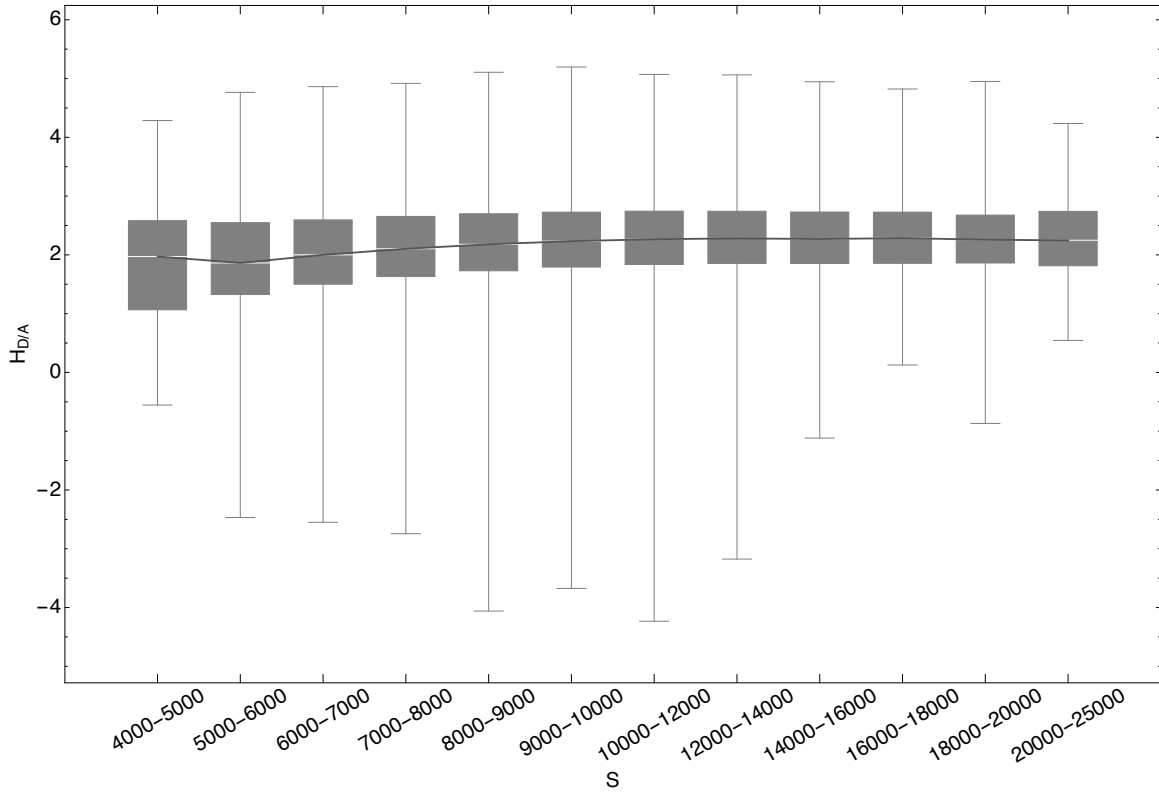
Supplementary Figure 4: The splicing variant rs10774671 is a strong asQTL for *OAS1*. Plotted is the normalized average coverage at which each base was sequenced along the genomic regions encoding the gene *OAS1*. Individuals were stratified according to their genotype at rs10774671. Below the figure are gene models from Ensembl database. Individuals carrying the G allele at rs10444671 (i.e., the Neandertal allele) primarily express the transcript ENST00000202917 (referred to as p46 in the text) whereas individuals carrying the A derived allele loose the splice site, which leads to the usage of a distinct isoform.

924  
925



926  
927 Supplementary Figure 5: Log 2 fold induction (y-axis) of *IFNA1* (type I  
928 interferon) and *IFNG* (type II interferon) in PBMCs upon infection/stimulation  
929 with several viral agents.

930  
931  
932  
933  
934  
935  
936  
937



938

939

940

941 Supplementary Figure 6:  $H_{D/A}$  does not vary substantially with SNP density.942  $H_{D/A}$  statistic plotted against number of segregating sites ( $S$ ) per locus across all943 neutral coalescent simulations. The slight increase in  $H_{D/A}$  with elevated  $S$  is944 conservative with respect to our one-tailed test for elevated  $H_{D/A}$ .

945

946

947

948

949

950

951

952

953

954

955

956

957

958

959

960

961

962

963

964 **Supplementary Tables:**  
 965  
 966

	CEU	GBR	IBS	TSI	Mathieson et al. 2015 P
113341598	0.856	0.407	0.967	0.256	0.233
113343563	0.862	0.428	0.529	0.524	0.335
113350796	0.0123	0.0194	0.395	0.0557	0.0249
113360025	0.00850	0.0114	0.0317	0.00633	0.000277
113363284	0.0126	0.0170	0.0288	0.00732	0.0000288
113370966	0.00654	0.00902	0.0190	0.00476	2.29E-08
113371114	0.00735	0.0102	0.0209	0.00518	0.000000315
113375983	0.00947	0.0140	0.0333	0.00787	0.00459
113435450	0.0167	0.0284	0.132	0.0409	0.0000375
113504725	0.0852	0.0797	0.134	0.0797	0.157
113532885	0.354	0.853	0.0112	0.218	0.0236
<b>p &lt;= 0.01</b>					
<b>0.01 &lt; p &lt;= 0.05</b>					

967  
 968 **Supplementary Table 1: Proportion of similar frequency genome-wide SNPs with**  
 969 **deviations from expected frequency as great or greater than 11 Neandertal-like**  
 970 **sites. Fraction of all non-OAS SNPs for which absolute difference in expected**  
 971 **(based on aDNA samples) and observed allele frequency that are as great or**  
 972 **greater than NLS derived allele frequency difference. Final column reports P from**  
 973 **Mathieson et al. 2015 selection test based on same aDNA samples.**  
 974  
 975